

# Breathing and rotobreathing cyclops states in phase oscillators with inertia and two-harmonic coupling

Matvei M. Khamkov<sup>1</sup>, Maxim I. Bolotov<sup>1</sup>, Lev A. Smirnov<sup>1</sup>, Igor Belykh<sup>2</sup>

<sup>1</sup>*Department of Control Theory,  
Lobachevsky State University of Nizhny Novgorod, 23 Gagarin Avenue,  
Nizhny Novgorod 603022, Russia*

<sup>2</sup>*Department of Mathematics and Statistics and Neuroscience Institute, Georgia State University,  
P.O. Box 4110, Atlanta, Georgia 30302-410, USA*

(Dated: May 13, 2026)

Cyclops states—three-cluster configurations consisting of two synchronous groups and a solitary oscillator—dominate in ensembles of phase oscillators with inertia and multiple coupling harmonics [Phys. Rev. E 109, 054202 (2024)]. In this work, for the first time, we systematically study nonstationary cyclops states that preserve the three-cluster structure: breathing and rotobreathing cyclops states. We identify two scenarios for their destabilization: period doubling, leading to quasicyclops states while preserving frequency synchronization within the clusters, and the destruction of one or two clusters, resulting in the emergence of switching cyclops or multicluster states. We show that breathing and rotobreathing cyclops states occupy vast parameter regions of the second coupling harmonic and are key elements of the dynamics. The results are important for predicting and controlling complex collective states in ensembles with higher-order interaction harmonics of various natures.

## I. INTRODUCTION

Networks of coupled phase oscillators are a universal tool for modeling collective dynamics in diverse systems—from neuronal ensembles and populations of chemical oscillators to laser arrays and power grids [1–5]. The classical first-order Kuramoto model and its extensions to oscillators with inertia [6–8] demonstrate a rich variety of states: full and partial synchronization [9, 10], chimera states [11–13], cluster structures [14, 15], and solitary states [16–18]. An important role in the formation of such states is played by higher harmonics of the coupling function, which naturally arise during the Fourier decomposition of an arbitrary periodic interaction function [19, 20]. Accounting for them allows one to describe effects such as the multiplicity of phase-locked states [21] and switching between clusters [22], which are inaccessible within the framework of the classical single-harmonic model.

In our recent work [23], a new class of three-cluster states termed cyclops states was introduced. Such states are formed by two coherent clusters and a single solitary oscillator, a configuration that, for an odd total number of elements, gives it a resemblance to the eye of a Cyclops. It was shown that in ensembles of oscillators with inertia and multiple coupling harmonics, cyclops states can dominate in a wide range of parameters, including regions of weak attraction and repulsion, and can even become global attractors when a second or third harmonic is added [23, 24]. This discovery stimulated further analysis of the stability and types of cyclops states.

In [24], a classification of cyclops states was proposed, distinguishing between stationary (with constant intercluster phase differences) and nonstationary states. Among the latter, breathing and rotobreathing cyclops states are of particular interest. In contrast to switching cyclops states, where the three-cluster configuration periodically dissolves and reforms with a reshuffling of oscillators, breathing and rotobreathing states preserve the three-cluster structure: in the first case, intercluster phase differences undergo bounded oscillations; in the second, they combine oscillations with rotation, leading to complex dynamics that preserves cluster integrity. In particular, it was shown [24] that breathing states can emerge as a result of an Andronov–Hopf bifurcation from stationary cyclops states. However, a detailed investigation of the breathing and rotobreathing states themselves—their internal structure, regions of existence, bifurcation mechanisms, and the role of higher harmonics—remained fragmentary within our works.

In parallel, the understanding of the role of inertia and heterogeneity has evolved. In [18], analytical conditions were obtained for the stability of rotatory solitary states, which serve as a prototype for the solitary oscillator in a cyclops state. Later, it was established that even a small heterogeneity in natural frequencies can stabilize cyclops and two-cluster states in parameter regions where they are unstable in the identical case [25]. These results emphasize that cyclops states are not an artifact of perfect symmetry but represent robust dynamical objects capable of emerging under realistic conditions.

The present work is devoted to a systematic analysis of breathing and rotobreathing cyclops states. We consider ensembles of phase oscillators with inertia and two harmonics in the coupling function, focusing on an odd number of elements, for which the cyclops configuration is preferential.

The paper is organized as follows. Section II provides a description of the model and a formulation of the problem. A reduction to a three-cluster manifold and the definitions of breathing and rotobreathing solutions are presented.

Section III presents an analysis of the existence and stability of breathing cyclops states, as well as scenarios for their destabilization. In Section IV, a similar analysis of rotobreathing solutions is performed. Section V presents a statistical analysis of the realizability of cyclops states. In the Conclusion, the obtained results are summarized, and directions for further research are outlined.

## II. MODEL. CYCLOPS STATES

We consider a network of  $N$  Kuramoto–Sakaguchi phase oscillators [26] with inertia and two harmonics in the coupling function, described by the equation:

$$\mu\ddot{\theta}_k + \dot{\theta}_k = \omega + \frac{1}{N} \sum_{n=1}^N \sum_{q=1}^2 \varepsilon_q \sin[q(\theta_n - \theta_k) - \alpha_q], \quad (1)$$

where  $\theta_k$  is the phase of the  $k$ th oscillator ( $k = 1, 2, \dots, N$ ), varying in the range  $-\pi < \theta_k \leq \pi$ . All oscillators are considered identical and are characterized by a natural frequency  $\omega$ , inertia  $\mu$ , phase lag parameters  $\alpha_1$  and  $\alpha_2$ , and coupling strength parameters  $\varepsilon_1$  and  $\varepsilon_2$  of the first and second harmonics, respectively. The two-harmonic coupling in the Kuramoto–Sakaguchi model is represented by the following interaction function:

$$H(\theta_n - \theta_k) = \sum_{q=1}^2 \varepsilon_q \sin[q(\theta_n - \theta_k) - \alpha_q]. \quad (2)$$

We consider a phase lag  $\alpha_1 \in (\frac{\pi}{2}, \pi]$ , which makes the coupling at the first harmonic repulsive, and fix  $\varepsilon_1 = 1$ , corresponding to a strong coupling. Throughout the paper, we also choose and fix a sufficiently strong inertia  $\mu = 1$ , which makes the dynamics of the 2D system qualitatively distinct from the 1D classical model, allowing the oscillatory dynamics of the clusters to be realized. We set the phase lag  $\alpha_2 \in (-\pi, \pi]$ , allowing the second harmonic to be either attractive or repulsive. As a result, the overall combined coupling can be repulsive when  $H'(0) < 0$  or attractive when  $H'(0) > 0$  [24]. The latter is possible if the second-harmonic coupling  $\varepsilon_2$  is sufficiently strong to overcome the contribution of the first harmonic coupling.

Phase coherence and cluster synchronization in system (1) can be characterized using the complex order parameters  $R_l$  [21]:

$$R_l(t) = \frac{1}{N} \sum_{k=1}^N e^{il\theta_k} = r_l e^{i\psi_l}, \quad (3)$$

where  $r_l$  and  $\psi_l$  determine the amplitude and phase of the  $l$ th moment order parameter  $R_l(t)$ , respectively. The parameter  $r_1 = |R_1|$  characterizes the degree of phase synchronization, where  $r_1 = 1$  corresponds to a fully synchronous state  $\theta_1 = \theta_2 = \dots = \theta_N$ . Splay states or generalized splay states  $\theta_k = \omega t + \varphi_k$  with constant nonuniform relative phases  $\varphi_k \in [-\pi, \pi]$  satisfy the condition  $r_1 = 0$  in the 2D Kuramoto model with the first harmonic in the coupling function ( $\varepsilon_2 = 0$ ) [23]. The parameter  $r_2 = |R_2|$  characterizes the degree of two-cluster separation, and the value  $r_2 = 1$  corresponds to a symmetric two-cluster state in a system with an even number of oscillators. In the case of single-harmonic coupling ( $\varepsilon_2 = 0$ ), the parameter  $r_2$  determines the stability of generalized splay states: larger stability regions on the parameter plane correspond to larger values of  $r_2$  [23]. In [23], it was shown that generalized splay states with a maximum  $r_2$  are:

- (a) two-cluster symmetric states with a cluster size  $N/2$  (for even  $N$ );
- (b) three-cluster states with relative phases (for odd  $N$ ):

$$\varphi_1 = \dots = \varphi_K = \gamma, \quad \varphi_M = 0, \quad \varphi_{M+1} = \dots = \varphi_N = -\gamma, \quad (4)$$

where  $\gamma = \arccos(1/(1-N))$ . In this state, two equal clusters of size  $K = (N-1)/2$  coexist with a solitary element with index  $M = (N+1)/2$ . The choice of the zero reference phase for  $\varphi_M$  is arbitrary. The three-cluster states (4) are termed cyclops states [23]. Adding the second-harmonic coupling with  $\varepsilon_2 \neq 0$  breaks their symmetry in  $\gamma$  and makes  $r_1$  nonzero, albeit small. In [23], it was shown that coupling with the second or higher harmonics can make these asymmetric structures dominant states. In [24], the following three-cluster state, defined by a three-dimensional cluster manifold:

$$D(3) = \begin{cases} \theta_1(t) = \dots = \theta_K(t) = \Omega t + x, \\ \theta_M(t) = \Omega t, \\ \theta_{M+1}(t) = \dots = \theta_N(t) = \Omega t + y \end{cases} \quad (5)$$

was identified as a stationary cyclops state in which all clusters rotate with a common frequency  $\Omega$ , maintaining stationary phase differences  $x = \gamma_1$  and  $y = \gamma_2$  with the  $M$ th solitary oscillator. A complete analysis of the existence and stability of stationary cyclops states was carried out in [24]. Here, we study in more detail nonstationary cyclops states in system (1). In the general case, these states can be described by a three-dimensional cluster manifold similarly to (5):

$$D(3) = \begin{cases} \theta_1(t) = \dots = \theta_K(t) = \psi(t) + x(t), \\ \theta_M(t) = \psi(t), \\ \theta_{M+1}(t) = \dots = \theta_N(t) = \psi(t) + y(t), \end{cases} \quad (6)$$

where  $\psi(t)$  describes the motion of the solitary oscillator, which is generally nonuniform. We call the nonstationary cyclops state (6) a **breathing** state if the conditions  $|x(t)| < \pi$  and  $|y(t)| < \pi$  are met. In such a state, the clusters oscillate relative to the solitary element without making phase slips relative to it. If  $|x(t)| > \pi$  or  $|y(t)| > \pi$ , the state is called **rotobreathing**. In this case, at least one of the clusters rotates relative to the solitary element.

Subtracting the equation for  $\theta_M$  from the remaining equations of (1), we obtain a reduced system describing the cluster phase-detuning dynamics  $x(t)$  and  $y(t)$  from the solitary element. Without loss of generality, we set the natural frequency of the oscillators  $\omega = 0$ . As a result, we obtain the following system of two second-order equations:

$$\begin{aligned} \mu \ddot{x} + \dot{x} &= \sum_{q=1}^2 \frac{\varepsilon_q}{N} \left[ \sin \alpha_q - \sin(qx + \alpha_q) - \frac{N-1}{2} \left( \sin(qx - \alpha_q) \right. \right. \\ &\quad \left. \left. + \sin(qy - \alpha_q) + \sin \alpha_q + \sin(q(x-y) + \alpha_q) \right) \right], \\ \mu \ddot{y} + \dot{y} &= \sum_{q=1}^2 \frac{\varepsilon_q}{N} \left[ \sin \alpha_q - \sin(qy + \alpha_q) - \frac{N-1}{2} \left( \sin(qy - \alpha_q) \right. \right. \\ &\quad \left. \left. + \sin(qx - \alpha_q) + \sin \alpha_q + \sin(q(y-x) + \alpha_q) \right) \right]. \end{aligned} \quad (7)$$

As was shown in [24], the equilibrium states of system (7) correspond to stationary cyclops states. When such a state loses stability due to an Andronov–Hopf bifurcation, a pair of complex-conjugate eigenvalues responsible for the stability of the intercluster phase differences crosses the imaginary axis, and a limit cycle is born, corresponding to a breathing cyclops: the clusters are preserved but begin to oscillate periodically with phases  $x(t)$  and  $y(t)$ . The temporal dynamics of the order parameters  $r_1(t)$  and  $r_2(t)$  also acquire an oscillatory character.

With a further change in the system parameters or an increase in the amplitude of the emerged oscillations, the phase detunings  $x(t)$  and  $y(t)$  can begin to make full  $2\pi$  rotations relative to the solitary oscillator. In this case, the state transforms into a rotobreathing cyclops state [24]. From the point of view of the reduced dynamical system (7), rotobreathers correspond to rotational trajectories in a cylindrical phase space. In such a state, the clusters not only periodically change their relative phase but also make one or more phase slips per period, which leads to more complex dynamics of the order parameters  $r_1(t)$  and  $r_2(t)$ .

For a more detailed geometric representation of the internal structure and destabilization mechanisms of nonstationary cyclops states, it is convenient to consider the projections of their phase trajectories onto the plane of relative cluster phase detunings  $(x_k, y_k)$ . Figure 1 presents typical projections for various states, a detailed analysis of the stability and bifurcations of which is given in the following sections.

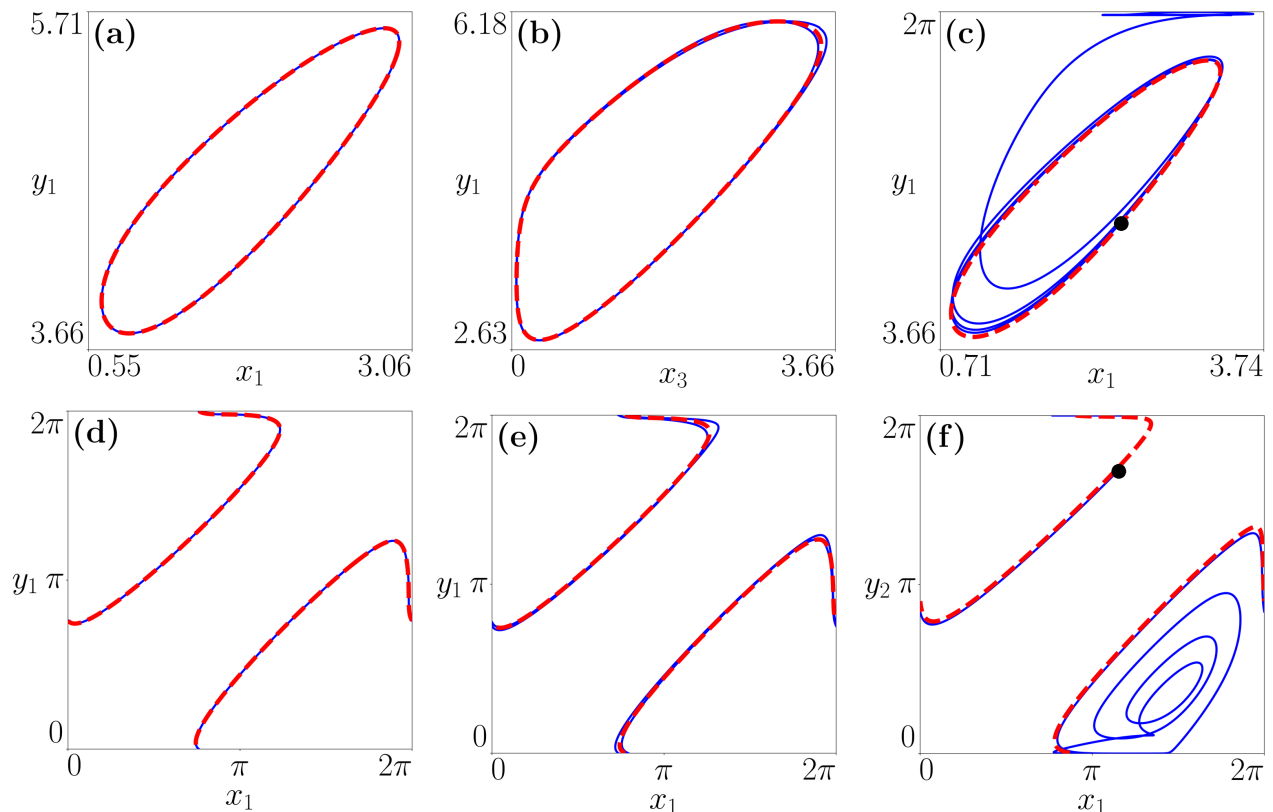


Figure 1. Projections of phase trajectories on the plane of relative cluster detunings  $(x_1, y_1)$ . Red dashed lines show trajectories from initial conditions found by the Newton–Raphson method. Solid blue lines represent established states started from nearby initial conditions. Black dots in panels (c) and (f) indicate the beginning of the blue trajectory. Upper row (breathing cyclops states): (a) the stable breathing cyclops at point A; (b) period doubling of the breathing cyclops at point B; (c) destabilization of the breathing cyclops at point C. Lower row (rotobreathing cyclops states): (d) the stable rotobreathing cyclops at point A; (e) period doubling of the rotobreathing cyclops at point B; (f) destabilization of the rotobreathing cyclops at point C. Parameters:  $N = 11$ ,  $\mu = 1.0$ ,  $\varepsilon_1 = 1.0$ ,  $\alpha_1 = 1.7$ . The values of  $\varepsilon_2$  and  $\alpha_2$  correspond to points A, B, C shown in Fig. 2 (panels (a)–(c)) and Fig. 6 (panels (d)–(f)).

### III. BREATHING CYCLOPS STATES

#### A. Existence of breathing cyclops states

Breathing cyclops states correspond to periodic trajectories in system (7). To detect them, we apply a modification of the widely used scheme for searching for closed trajectories in nonlinear dynamical systems. We denote the solution of system (7) as  $\mathbf{F}(t, \mathbf{X}_0) = (x(t, \mathbf{X}_0), \dot{x}(t, \mathbf{X}_0), y(t, \mathbf{X}_0), \dot{y}(t, \mathbf{X}_0))$ , where  $\mathbf{X}_0 = (x_0, \dot{x}_0, y_0, \dot{y}_0)$  is a point in the phase space corresponding to the initial conditions. Let  $\mathbf{F}_p(t, \mathbf{X}_0^{(p)})$  be the sought periodic solution with period  $T$ :  $\mathbf{F}_p(t + T, \mathbf{X}_0^{(p)}) = \mathbf{F}_p(t, \mathbf{X}_0^{(p)})$ , where  $\mathbf{X}_0^{(p)}$  is a point lying on the periodic trajectory. We consider the map describing the system-state evolution over the time period  $T$ , which is, generally speaking, unknown and requires determination:

$$\mathbf{P} : \mathbf{X}_n \rightarrow \mathbf{X}_{n+1}, \quad (8)$$

where  $\mathbf{X}_{n+1} = \mathbf{F}(T, \mathbf{X}_n)$ . Any point lying on the periodic trajectory  $\mathbf{F}_p(t, \mathbf{X}_0^{(p)})$  is a fixed point of this map. Using the periodicity conditions, we construct a system of nonlinear equations:

$$\mathbf{G}(t, \mathbf{X}) = \mathbf{F}(t, \mathbf{X}) - \mathbf{F}(0, \mathbf{X}) = 0. \quad (9)$$

The root of this equation is the vector  $(T, \mathbf{X}_0^{(p)})$ , where  $T$  is the period and  $\mathbf{X}_0^{(p)}$  is the coordinate of a point lying on the sought periodic trajectory. Due to the closedness of the trajectory, we fix one of the values in the set  $\{x, \dot{x}, y, \dot{y}\}$ ,

for example  $x$ , which makes system (9) solvable. To find an approximate solution, we apply the Newton–Raphson iterative algorithm. As a result, we numerically obtain the initial conditions for the sought trajectory  $\mathbf{F}_p(t, \mathbf{X}_0^{(p)})$ .

### B. Linear stability analysis of breathing cyclops states

We conduct a stability analysis of the found periodic trajectories. We write system (1) using (2):

$$\mu\ddot{\theta}_k + \dot{\theta}_k = \frac{1}{N} \sum_{n=1}^N H(\theta_n - \theta_k). \quad (10)$$

We consider the phase detunings of the cluster elements  $x_i$  and  $y_i$  relative to the solitary oscillator:

$$x_i = \theta_i - \theta_M, \quad y_i = \theta_{M+i} - \theta_M, \quad i = 1, \dots, K. \quad (11)$$

We obtain a system of  $2K$  equations:

$$\begin{aligned} \mu\ddot{x}_i + \dot{x}_i &= \frac{1}{N} \left[ H(-x_i) + \sum_{j=1}^K H(x_j - x_i) + \sum_{j=1}^K H(y_j - x_i) \right. \\ &\quad \left. - H(0) - \sum_{j=1}^K H(x_j) - \sum_{j=1}^K H(y_j) \right], \\ \mu\ddot{y}_i + \dot{y}_i &= \frac{1}{N} \left[ H(-y_i) + \sum_{j=1}^K H(x_j - y_i) + \sum_{j=1}^K H(y_j - y_i) \right. \\ &\quad \left. - H(0) - \sum_{j=1}^K H(x_j) - \sum_{j=1}^K H(y_j) \right]. \end{aligned} \quad (12)$$

To study the linear stability of cyclops states in system (12), we consider small perturbations relative to the phase detunings  $x(t)$  and  $y(t)$ :

$$x_i(t) = x(t) + \delta x_i(t); \quad y_i(t) = y(t) + \delta y_i(t).$$

Linearizing system (12) in their vicinity, we obtain the following equations:

$$\begin{aligned} \mu\delta\ddot{x}_i + \delta\dot{x}_i &= \frac{1}{N} \left[ -A_x(x, y)\delta x_i + B_x(x) \sum_{j=1}^K \delta x_j + C_x(x, y) \sum_{j=1}^K \delta y_j \right], \\ \mu\delta\ddot{y}_i + \delta\dot{y}_i &= \frac{1}{N} \left[ -A_y(x, y)\delta y_i + B_y(y) \sum_{j=1}^K \delta y_j + C_y(x, y) \sum_{j=1}^K \delta x_j \right], \end{aligned} \quad (13)$$

where:

$$\begin{aligned} A_x(x, y) &= H'(-x) + KH'(0) + KH'(y - x), \\ B_x(x) &= H'(0) - H'(x), \quad C_x(x, y) = H'(y - x) - H'(y), \\ A_y(x, y) &= H'(-y) + KH'(0) + KH'(x - y), \\ B_y(y) &= H'(0) - H'(y), \quad C_y(x, y) = H'(x - y) - H'(x). \end{aligned}$$

Next, we use Floquet analysis. System (13) can be represented in a space of dimension  $4K$  as:

$$\delta\dot{\mathbf{Z}} = \mathbf{J}(t)\delta\mathbf{Z}, \quad (14)$$

where:

$$\delta\mathbf{Z} = (\delta x_1, \delta \dot{x}_1, \dots, \delta x_K, \delta \dot{x}_K, \delta y_1, \delta \dot{y}_1, \dots, \delta y_K, \delta \dot{y}_K)$$

is the vector combining all phase variables and velocities,

$$\mathbf{J}(t) = \left[ \begin{array}{cc} \mathbf{I}_K \otimes \mathbf{D}_1(x, y) + (\mathbf{E}_K - \mathbf{I}_K) \otimes \mathbf{D}_2(x) & \mathbf{E}_K \otimes \mathbf{D}_3(x, y) \\ \mathbf{E}_K \otimes \mathbf{D}_4(x, y) & \mathbf{I}_K \otimes \mathbf{D}_5(x, y) + (\mathbf{E}_K - \mathbf{I}_K) \otimes \mathbf{D}_6(y) \end{array} \right] \Big|_{\mathbf{X}=\mathbf{F}_p(t, \mathbf{X}_0^{(p)})}$$

is the functional matrix of period  $T$ , where  $\mathbf{I}_K \in \mathbb{R}^{K \times K}$  is the identity matrix,  $\mathbf{E}_K \in \mathbb{R}^{K \times K}$  is a matrix filled with ones, the symbol  $\otimes$  denotes the Kronecker product, and the blocks  $\mathbf{D}_j \in \mathbb{R}^{2 \times 2}$ ,  $j = 1, 2, \dots, 6$  have the form:

$$\begin{aligned} \mathbf{D}_1(x, y) &= \begin{bmatrix} 0 & 1 \\ (\mu N)^{-1}(B_x(x) - A_x(x, y)) & -\mu^{-1} \end{bmatrix}, & \mathbf{D}_2(x) &= \begin{bmatrix} 0 & 0 \\ (\mu N)^{-1}B_x(x) & 0 \end{bmatrix}, \\ \mathbf{D}_3(x, y) &= \begin{bmatrix} 0 & 0 \\ (\mu N)^{-1}C_x(x, y) & 0 \end{bmatrix}, & \mathbf{D}_4(x, y) &= \begin{bmatrix} 0 & 0 \\ (\mu N)^{-1}C_y(x, y) & 0 \end{bmatrix}, \\ \mathbf{D}_5(x, y) &= \begin{bmatrix} 0 & 1 \\ (\mu N)^{-1}(B_y(y) - A_y(x, y)) & -\mu^{-1} \end{bmatrix}, & \mathbf{D}_6(y) &= \begin{bmatrix} 0 & 0 \\ (\mu N)^{-1}B_y(y) & 0 \end{bmatrix}. \end{aligned}$$

The fundamental matrix  $\Phi(t)$  of system (14) satisfies the equation  $\dot{\Phi}(t) = \mathbf{J}(t)\Phi(t)$  with the initial condition  $\Phi(0) = \mathbf{I}_{4K}$ . The evolution of an arbitrary initial perturbation  $\delta\mathbf{Z}(0)$  over one period  $T$  is determined by the monodromy matrix  $\Phi(T)$ :

$$\delta\mathbf{Z}(T) = \Phi(T) \delta\mathbf{Z}(0). \quad (15)$$

The eigenvalues  $\lambda_j$  ( $j = 1, \dots, 4K$ ) of the monodromy matrix  $\Phi(T)$  are called Floquet multipliers. Due to the closedness of the investigated trajectory, one of the eigenvalues  $\lambda_{4K}$  is always equal to 1. The periodic solution  $\mathbf{F}_p(t, \mathbf{X}_0^{(p)})$  is stable if the remaining multipliers lie inside the unit circle, i.e.,  $|\lambda_j| < 1$  for all  $j < 4K$ . The presence of at least one multiplier with  $|\lambda_j| > 1$  indicates linear instability. We denote the maximum modulus eigenvalue (not equal to one) as  $\lambda_{\max}$ , which characterizes the destabilization of periodic states:

$$\lambda_{\max} = \lambda_{i^*}, \quad \text{where } i^* = \underset{j=1, \dots, 4K-1}{\operatorname{argmax}} |\lambda_j|. \quad (16)$$

### C. Stable breathing cyclops states

To determine the boundaries of existence and stability of breathing cyclops states on the parameter plane  $(\alpha_2, \varepsilon_2)$ , a continuous parameter continuation method was applied. For each fixed set of parameters, Eq. (9) was solved, and the stability of the found periodic trajectories was investigated using Floquet analysis (15). The state map obtained in this way for the parameters  $N = 11$ ,  $\mu = 1.0$ ,  $\varepsilon_1 = 1.0$ ,  $\alpha_1 = 1.7$  is presented in Fig. 2. The parameter value  $\alpha_1 = 1.7$  was chosen in accordance with the results of work [24], where it was shown that the greatest variety of cyclops states is observed at this value. The regions of parameters where a stable breathing cyclops exists are marked in blue on the map, and the regions where a periodic solution exists but is unstable are marked in red. The stability region boundaries are determined by the periodic-motion bifurcation type: the continuous black line corresponds to the loss of stability when the Floquet multiplier (16) crosses the value  $\lambda_{\max} = -1$ , and the dashed black line—when crossing  $\lambda_{\max} = 1$ .

The boundary of existence of the breathing cyclops states is formed by the following curves: (i) the Andronov–Hopf bifurcation curve giving rise to a limit cycle from an equilibrium state—the gray curve with black filled circular markers; (ii) the saddle-node bifurcation curve of the limit cycle, when two limit cycles merge and disappear—the gray curve with black open circular markers; and (iii) the homoclinic bifurcation curve of the limit cycle, when the limit cycle merges with the saddle separatrix, forming a homoclinic loop, after which the cycle disappears—the gray curve with black cross markers (Fig. 2). In the first case, the clusters' oscillation amplitude relative to the solitary element gradually decays, which leads to the emergence of a stationary cyclops state; in the second case, the breathing state disappears with a finite oscillation amplitude; and in the third case, the period of oscillations increases indefinitely.

As an example of a stable breathing cyclops state, we consider the dynamics of the system at point  $A$  (Fig. 2) with parameters  $\varepsilon_2 = 0.049$  and  $\alpha_2 = -0.377$ , lying inside the stability region. At this point, the projection of the phase trajectory is a stable limit cycle (Fig. 1a). The results of numerical integration of the initial system (1) are presented in Fig. 3. The diagram of phase differences (Fig. 3a) shows that the system reaches a stable breathing cyclops state: the oscillators in each of the two clusters move synchronously in phase, making periodic oscillations relative to the solitary oscillator, while the amplitude of these oscillations does not exceed the value of  $\pi$ . The Floquet multiplier map (Fig. 3b) confirms the stability of the state.

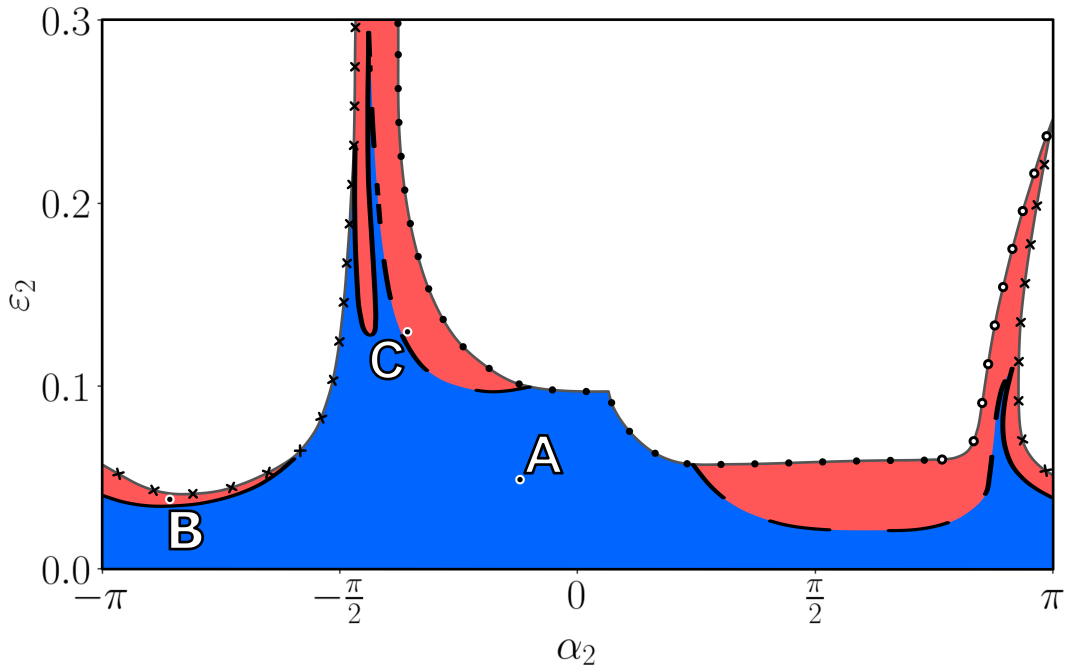


Figure 2. Region of existence of **breathing cyclops states**. Blue and red indicate stability and instability regions, respectively. The continuous black line marks the stability boundary where  $\lambda_{\max} = -1$ , and the dashed black line where  $\lambda_{\max} = 1$ . Gray curves with black markers indicate bifurcation curves: solid circles – Andronov–Hopf; open circles – saddle-node of the limit cycle; crosses – homoclinic of the limit cycle. Parameters:  $N = 11$ ,  $\mu = 1.0$ ,  $\varepsilon_1 = 1.0$ ,  $\alpha_1 = 1.7$ .

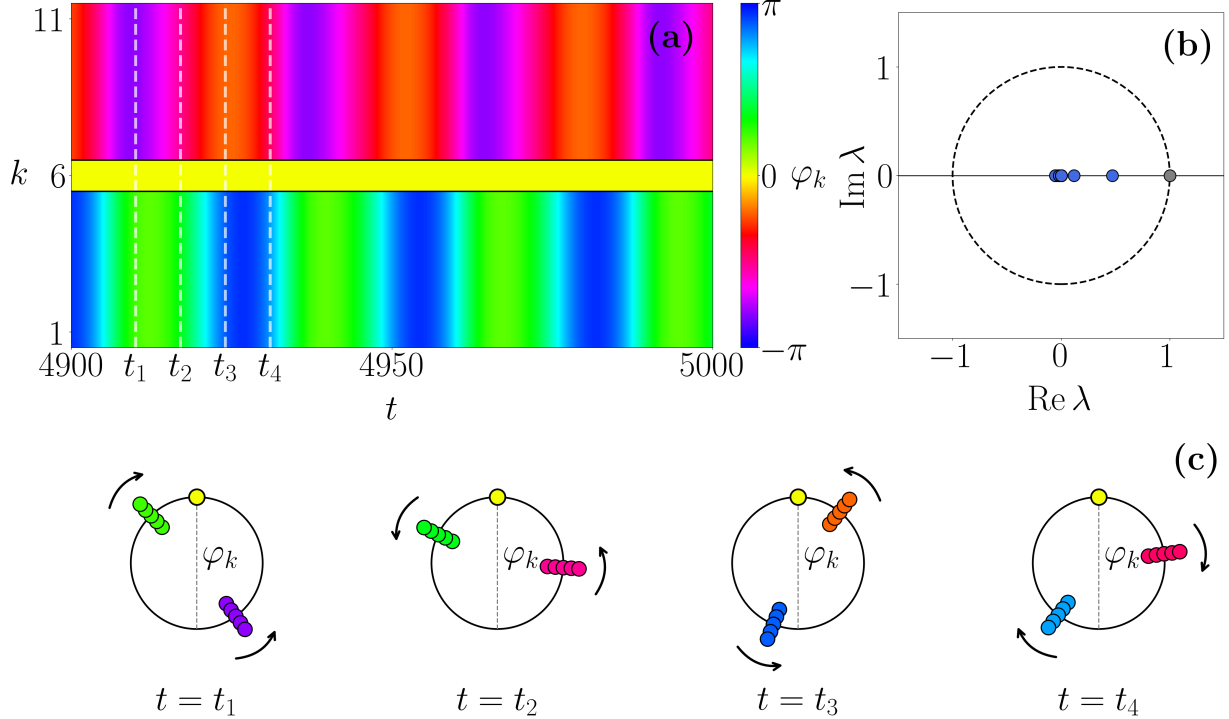


Figure 3. A stable breathing cyclops state: (a) diagram of the phase differences between the oscillators and the solitary element ( $\varphi_k = \theta_k - \theta_6$ ); (b) Floquet multipliers on the complex plane (blue dots: stable  $\lambda_j$ ; gray dot:  $\lambda_{4K} = 1$ ); (c) snapshots of the instantaneous phases of the oscillators at time moments  $t_1 = 4910$ ,  $t_2 = 4917$ ,  $t_3 = 4924$ ,  $t_4 = 4931$ , with arrows indicating the direction of motion. Parameters:  $N = 11$ ,  $\mu = 1.0$ ,  $\varepsilon_1 = 1.0$ ,  $\alpha_1 = 1.7$ ,  $\varepsilon_2 = 0.049$ ,  $\alpha_2 = -0.377$ .

### D. Destabilization of the breathing cyclops state

We consider the dynamics of the system at points on the parameter plane where the breathing cyclops, according to the results of the Floquet analysis, is unstable. Depending on how exactly the multiplier leaves the unit circle, different scenarios for the destruction of the structure of the breathing cyclops are realized.

At point  $B$  (Fig. 2) with parameters  $\varepsilon_2 = 0.0346$  and  $\alpha_2 = -2.765$ , the Floquet multiplier crosses the value  $\lambda_{\max} = -1$ , which corresponds to a period-doubling bifurcation. In Fig. 1b, the unstable cycle obtained from exact initial conditions is shown in red, while the established trajectory with a doubled period, which emerged after introducing a small perturbation, is shown in blue. The results of numerical integration of system (1) are presented in Fig. 4. On the phase snapshots for time moments  $t_3$  and  $t_4$  (Fig. 4c), it can be seen that the initial breathing cyclops loses stability; however, complete destruction of the cluster structure does not occur. The system transitions to a multicluster breathing **quasicyclops state** with a doubled period, while the newly formed clusters are preserved, and the amplitude of the oscillations of the oscillators within them does not exceed  $\pi$  in modulus. The Floquet multiplier map (Fig. 4b) demonstrates the exit of one of the multipliers outside the unit circle via  $-1$ . On the color diagram (Fig. 4a), this period-doubling effect is visually weakly expressed, which is due to the proximity of the unstable eigenvalue to the stability boundary, because of which the amplitude of the phase splitting inside the clusters remains extremely small. It is not possible to capture a more visual dynamics with a pronounced period doubling: with a further change in parameters deep into the instability region, the breathing state completely breaks down, and the system transitions to a stable rotobreathing state.

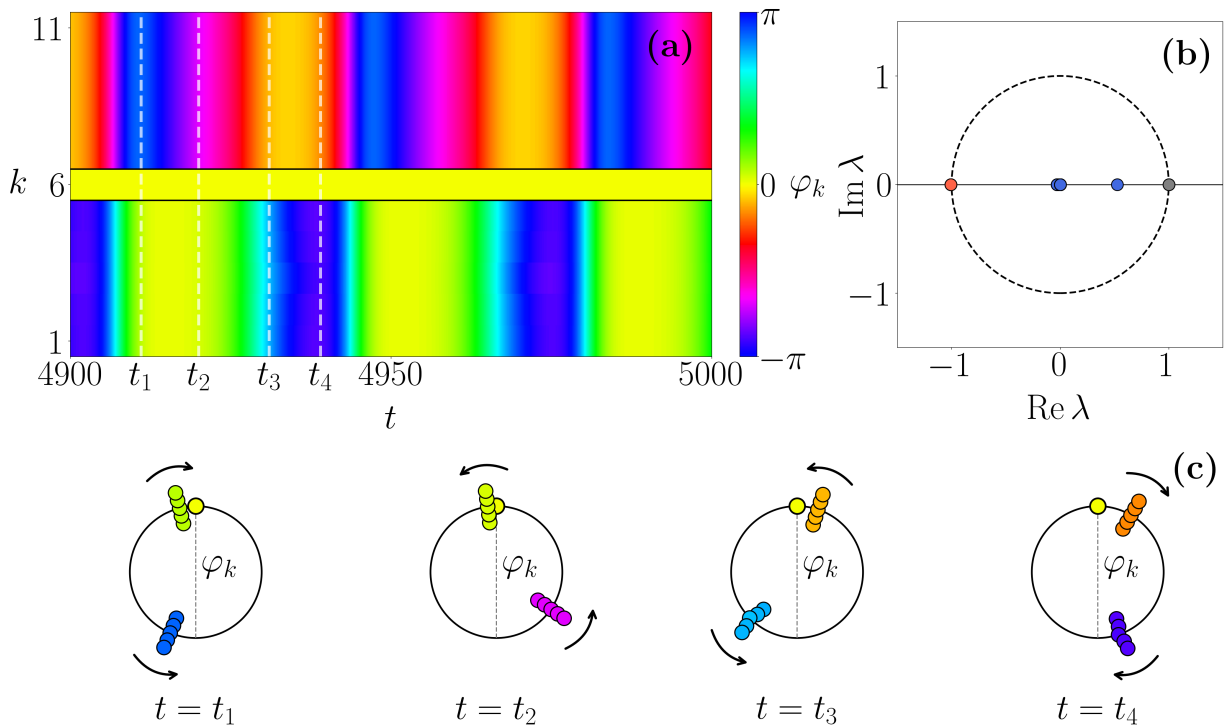


Figure 4. A breathing quasicyclops state with a doubled period: (a) diagram of the phase differences between the oscillators and the solitary element ( $\varphi_k = \theta_k - \theta_6$ ); (b) Floquet multipliers on the complex plane (blue dots: stable multipliers; red dot: unstable multiplier; gray dot: trivial multiplier  $\lambda_{4K} = 1$ ); (c) snapshots of the instantaneous phases of the oscillators at time moments  $t_1 = 4911$ ,  $t_2 = 4920$ ,  $t_3 = 4931$ ,  $t_4 = 4939$ , with arrows indicating the direction of motion. Parameters:  $N = 11$ ,  $\mu = 1.0$ ,  $\varepsilon_1 = 1.0$ ,  $\alpha_1 = 1.7$ ,  $\varepsilon_2 = 0.0346$ ,  $\alpha_2 = -2.765$ .

A different scenario is observed at point  $C$  (Fig. 2) with parameters  $\varepsilon_2 = 0.13$  and  $\alpha_2 = -1.169$ , where the multiplier crosses the value  $\lambda_{\max} = 1$ . The original cycle thus loses stability: the perturbed trajectory (Fig. 1c, blue line) demonstrates the destruction of the breathing structure and the departure of the system into a switching cyclops state [24]. On the diagram (Fig. 5a), one can observe how the solitary element synchronizes with a coherent group, destabilizing one of its elements, which becomes the new solitary oscillator. The Floquet multiplier map (Fig. 5b) confirms the presence of instability.

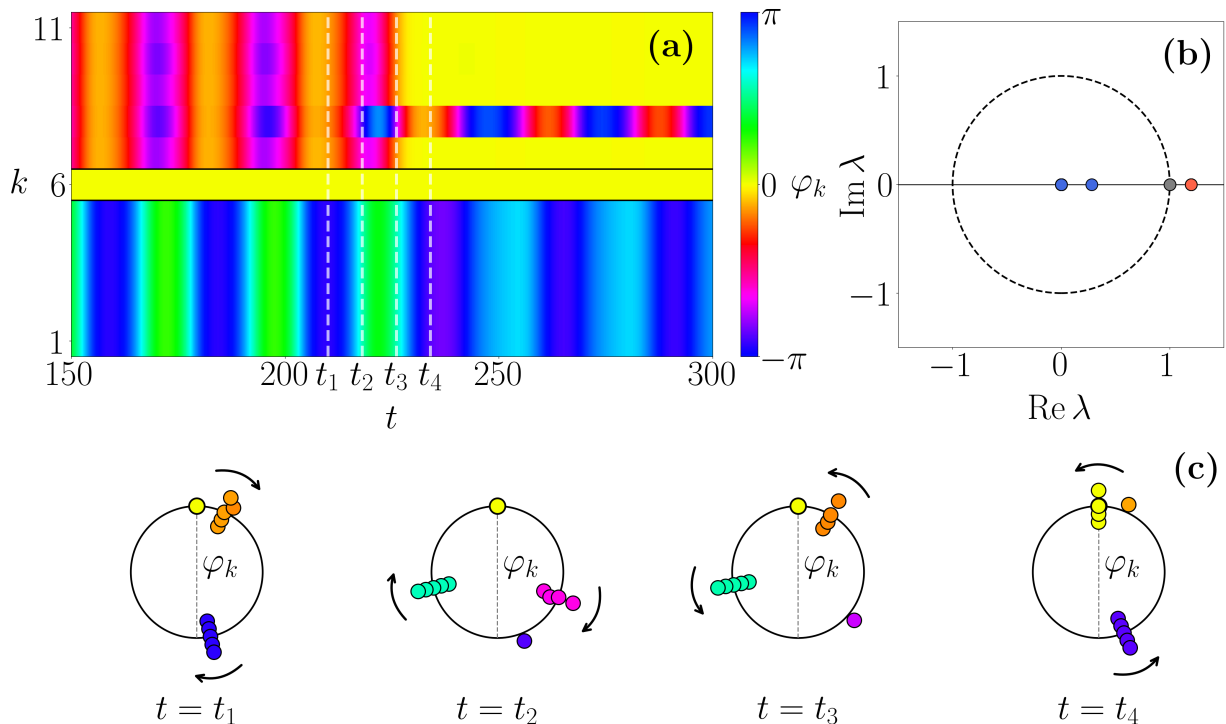


Figure 5. Destruction of a breathing cyclops state leading to a switching cyclops state: (a) diagram of the phase differences between the oscillators and the solitary element ( $\varphi_k = \theta_k - \theta_6$ ); (b) Floquet multipliers on the complex plane (blue dots: stable multipliers; red dot: unstable multiplier; gray dot: trivial multiplier  $\lambda_{4K} = 1$ ); (c) snapshots of the instantaneous phases of the oscillators at time moments  $t_1 = 210$ ,  $t_2 = 218$ ,  $t_3 = 226$ ,  $t_4 = 234$ , with arrows indicating the direction of motion. Parameters:  $N = 11$ ,  $\mu = 1.0$ ,  $\varepsilon_1 = 1.0$ ,  $\alpha_1 = 1.7$ ,  $\varepsilon_2 = 0.13$ ,  $\alpha_2 = -1.169$ .

## IV. ROTOBREATHING CYCLOPS STATES

### A. Existence and stability of rotobreathing cyclops states

In contrast to breathing states, rotobreathing cyclops states correspond to rotatory trajectories in system (7), for which at least one of the phase detunings  $x(t)$  or  $y(t)$  makes full revolutions of  $2\pi$  relative to the solitary element. To search for such states, a modification of the method used for breathing cyclops states is applied, taking into account the rotational nature of the motion. Let  $\mathbf{F}_r(t, \mathbf{X}_0^{(r)})$  be the sought rotatory solution, which, in addition to the period  $T$ , is characterized by the numbers of full revolutions  $n$  and  $m$  of the phases  $x(t)$  and  $y(t)$  during this time:

$$\mathbf{F}_r(t + T, \mathbf{X}_0^{(r)}) = \mathbf{F}_r(t, \mathbf{X}_0^{(r)}) + (2\pi n, 0, 2\pi m, 0), \quad (17)$$

where  $\mathbf{X}_0^{(r)}$  is a point lying on the rotatory trajectory. We consider the Poincaré map describing the evolution of the system's state over the time period  $T$  accounting for the rotation:

$$\mathbf{P} : \mathbf{X}_n \rightarrow \mathbf{X}_{n+1}, \quad (18)$$

where  $\mathbf{X}_{n+1} = \mathbf{F}(T, \mathbf{X}_n) - (2\pi n, 0, 2\pi m, 0)$ . Any point  $\mathbf{X}_0^{(r)}$  lying on the rotatory trajectory is a fixed point of this map. Using the periodicity conditions (17), we construct a system of nonlinear equations:

$$\mathbf{R}(t, \mathbf{X}) = \mathbf{F}(t, \mathbf{X}) - \mathbf{F}(0, \mathbf{X}) - (2\pi n, 0, 2\pi m, 0) = 0. \quad (19)$$

The root of this equation is the vector  $(T, \mathbf{X}_0^{(r)})$ , where  $T$  is the period and  $\mathbf{X}_0^{(r)}$  is the coordinate of a point lying on the sought rotatory trajectory. Due to the closedness of the trajectory on the cylinder, one of the values in the set  $\{x, y\}$  can be set to zero without loss of generality, for example  $x = 0$ , which makes system (19) solvable. To search for rotobreathing states in the present work, single-turn rotatory trajectories with  $n = m = -1$  are considered. The

Newton–Raphson iterative algorithm is applied to find the solution. As a result, the sought trajectory  $\mathbf{F}_r(t, \mathbf{X}_0^{(r)})$  is obtained numerically.

The linear stability analysis of the rotobreathing cyclops states is performed similarly to the case of breathing cyclops states using Floquet analysis. The variational system (13) remains valid for rotatory trajectories, since it is obtained by linearizing the original equations without assuming the bounded nature of the phase detunings. The stability of the rotobreathing state is determined by the position of the Floquet multipliers relative to the unit circle, with one of the multipliers always equal to unity due to the closedness of the trajectory  $\mathbf{F}_r(t, \mathbf{X}_0^{(r)})$  on the cylinder.

### B. Stable rotobreathing cyclops states

To determine the boundaries of existence and stability of rotobreathing cyclops states on the parameter plane  $(\alpha_2, \varepsilon_2)$ , a parameter continuation method was applied. For each fixed set of parameters, Eq. (19) was solved, and the stability of the found rotatory trajectories was investigated using Floquet analysis. The state map obtained for the parameters  $N = 11$ ,  $\mu = 1.0$ ,  $\varepsilon_1 = 1.0$ ,  $\alpha_1 = 1.7$  is presented in Fig. 6. The regions of parameters where a stable rotobreathing cyclops exists are marked in blue on the map, and the regions where a rotatory solution exists but is unstable are marked in red. The stability region boundaries, as in the case of breathers, are determined by the type of bifurcation: the continuous black line corresponds to the loss of stability when the Floquet multiplier crosses the value  $\lambda_{\max} = -1$ , and the dashed black line—when  $\lambda_{\max} = 1$ .

The boundary of existence of the rotobreathing cyclops states is formed by the homoclinic bifurcation curve, when the rotatory trajectory merges with the saddle separatrix, forming a homoclinic loop, after which it disappears—the gray curve with black cross markers (Fig. 6). When approaching this curve, the rotation period increases indefinitely.

As an example of a stable rotobreathing state, we consider the dynamics of the system at point *A* in Fig. 6 with parameters  $\varepsilon_2 = 0.08$  and  $\alpha_2 = -2.704$ , lying inside the stability region. The projection of the phase trajectory for this state is rotatory on the cylinder, completing a full circuit along both coordinates per period (Fig. 1d). The results of numerical integration of the original system (1) from initial conditions close to the found rotatory solution  $\mathbf{X}_0^{(r)}$  are presented in Fig. 7. On the diagram of phase differences (Fig. 7a), it can be seen that the oscillators in each of the two clusters move synchronously, making periodic rotations relative to the solitary oscillator, which corresponds to the definition of a rotobreathing state. The Floquet multiplier map (Fig. 7b) confirms the stability of the state.

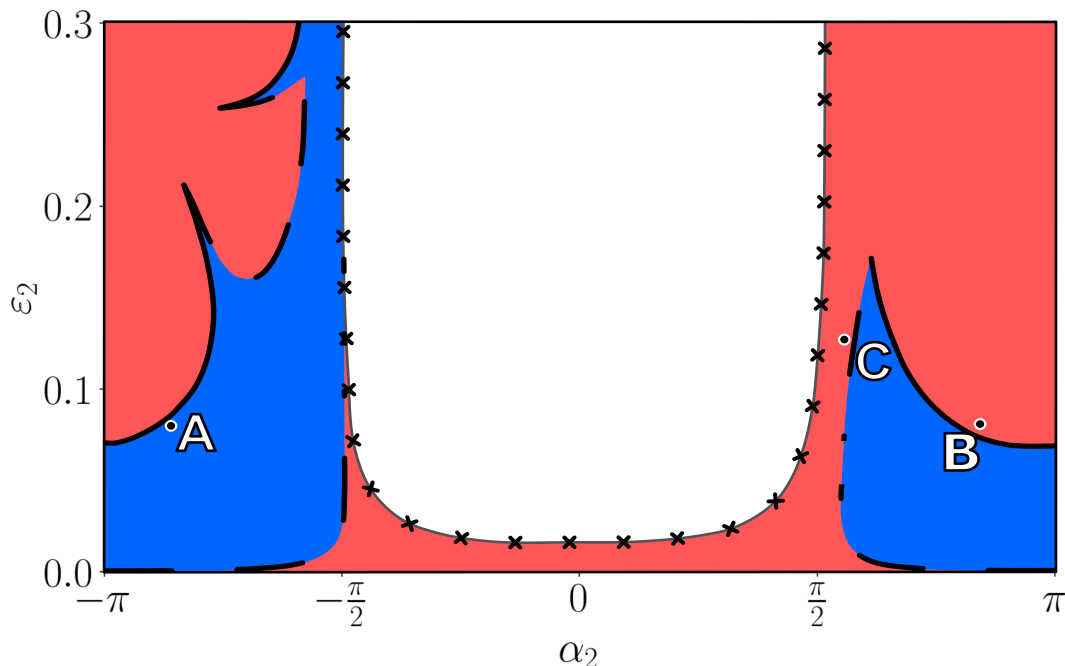


Figure 6. Region of existence of **rotobreathing cyclops states**. Blue and red indicate stability and instability regions, respectively. The continuous black line marks the stability boundary where  $\lambda_{\max} = -1$ , and the dashed black line where  $\lambda_{\max} = 1$ . The gray curve with black cross markers indicates the homoclinic bifurcation curve of the limit cycle. Parameters:  $N = 11$ ,  $\mu = 1.0$ ,  $\varepsilon_1 = 1.0$ ,  $\alpha_1 = 1.7$ .

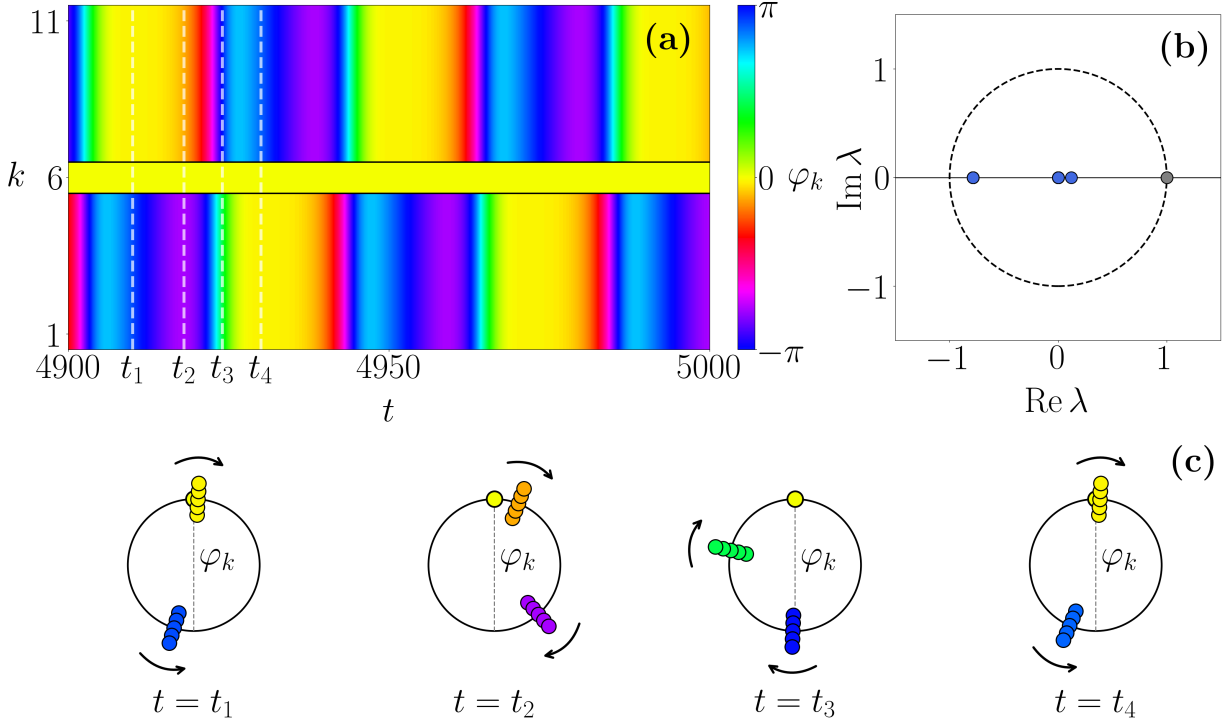


Figure 7. A stable rotobreathing cyclops state: (a) diagram of the phase differences between the oscillators and the solitary element ( $\varphi_k = \theta_k - \theta_6$ ); (b) Floquet multipliers on the complex plane (blue dots: stable multipliers; gray dot: trivial multiplier  $\lambda_{4K} = 1$ ); (c) snapshots of the instantaneous phases of the oscillators at time moments  $t_1 = 4910$ ,  $t_2 = 4918$ ,  $t_3 = 4924$ ,  $t_4 = 4930$ , with arrows indicating the direction of motion. Parameters:  $N = 11$ ,  $\mu = 1.0$ ,  $\varepsilon_1 = 1.0$ ,  $\alpha_1 = 1.7$ ,  $\varepsilon_2 = 0.08$ ,  $\alpha_2 = -2.704$ .

### C. Destabilization of the rotobreathing cyclops state

We consider the dynamics of the system at points on the parameter plane  $(\alpha_2, \varepsilon_2)$  where the rotobreathing cyclops, according to the results of the Floquet analysis, is unstable. As in the case of breathers, the character of the structure's destruction depends on exactly which multiplier leaves the unit circle.

At point *B* (Fig. 6) with parameters  $\varepsilon_2 = 0.08$  and  $\alpha_2 = 2.65$ , the Floquet multiplier crosses the value  $\lambda_{\max} = -1$ . The loss of stability leads to a period doubling of the rotatory motion, which manifests itself in the formation of a double loop on the phase portrait (Fig. 1e, blue line). Numerical integration of system (1) shows that the rotobreathing cyclops loses stability, but the system transitions to a multicluster **rotobreathing quasicyclops state** with a doubled period, which remains stable (Fig. 8a). The newly formed clusters demonstrate stability, while making periodic rotations relative to the solitary element with a period twice the original. The Floquet multiplier map (Fig. 8b) confirms the loss of stability via  $-1$ .

A different scenario is observed at point *C* (Fig. 6) with parameters  $\varepsilon_2 = 0.129$  and  $\alpha_2 = 1.72$ , where the multiplier crosses the value  $\lambda_{\max} = 1$ . This transition causes destabilization of the rotobreather, at which the perturbed trajectory (Fig. 1f, blue line) transitions to switching dynamics. The rotobreathing cyclops loses stability, and a switching cyclops state emerges [24]. On the diagram, one can observe how the solitary element synchronizes with a coherent group, destabilizing one of its elements, which becomes the new solitary oscillator (Fig. 9a). The Floquet multiplier map (Fig. 9b) confirms the presence of instability.

## V. PERSISTENCE OF CYCLOPS STATES

In addition to the analysis of the stability regions of breathing and rotobreathing cyclops states, a statistical analysis was performed, showing a high probability of realizing that states under random initial conditions. Figure 10 presents the dependences of the probability  $P$  of realizing various types of dynamical states on the phase shift  $\alpha_2$  for a fixed coupling strength of the second harmonic  $\varepsilon_2$ . The probability was calculated based on the numerical integration of

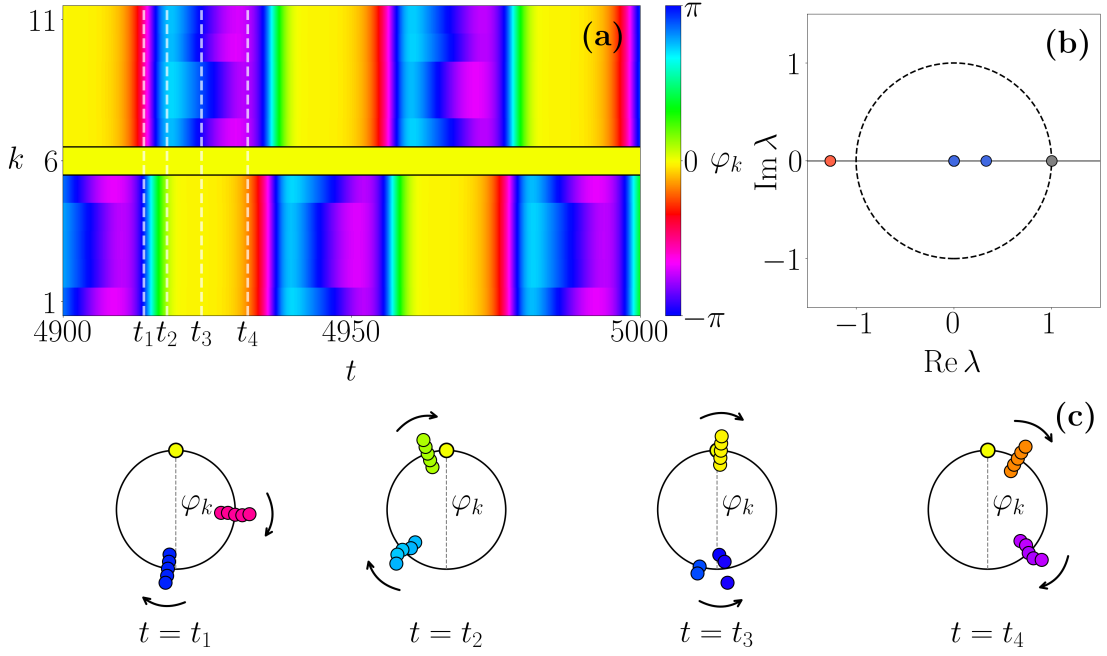


Figure 8. A rotobreathing quasicyclops state with a doubled period: (a) diagram of the phase differences between the oscillators and the solitary element ( $\varphi_k = \theta_k - \theta_6$ ); (b) Floquet multipliers on the complex plane (blue dots: stable multipliers; red dot: unstable multiplier; gray dot: trivial multiplier  $\lambda_{4K} = 1$ ); (c) snapshots of the instantaneous phases of the oscillators at time moments  $t_1 = 4914$ ,  $t_2 = 4918$ ,  $t_3 = 4924$ ,  $t_4 = 4932$ , with arrows indicating the direction of motion. Parameters:  $N = 11$ ,  $\mu = 1.0$ ,  $\varepsilon_1 = 1.0$ ,  $\alpha_1 = 1.7$ ,  $\varepsilon_2 = 0.08$ ,  $\alpha_2 = 2.65$ .

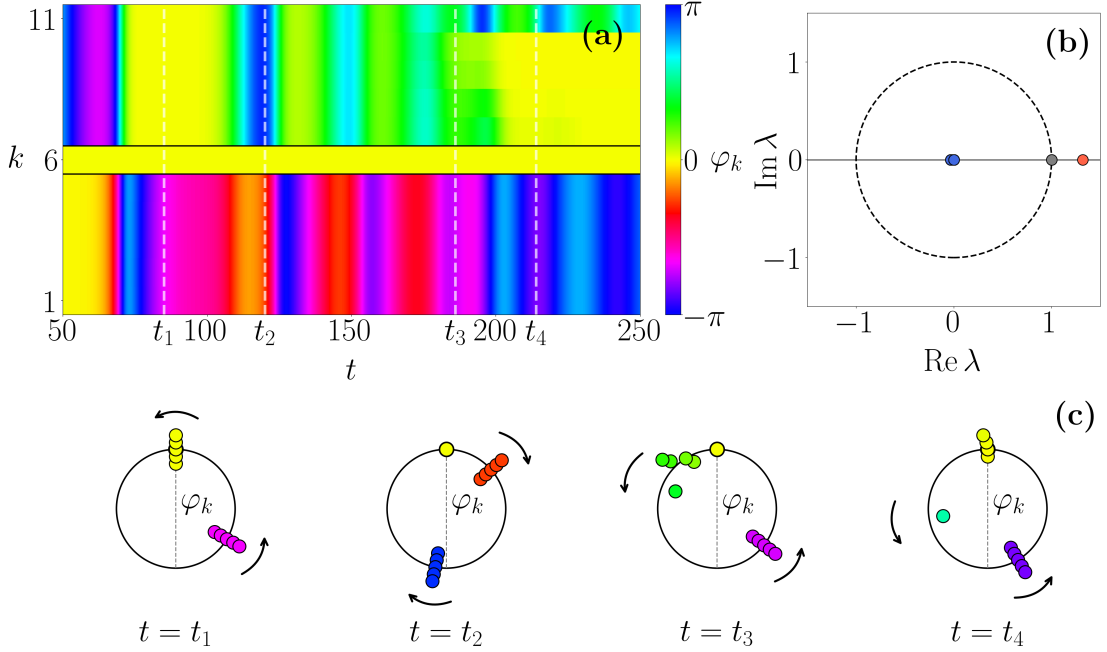


Figure 9. Destruction of a rotobreathing cyclops state leading to a switching cyclops state: (a) diagram of the phase differences between the oscillators and the solitary element ( $\varphi_k = \theta_k - \theta_6$ ); (b) Floquet multipliers on the complex plane (blue dots: stable multipliers; red dot: unstable multiplier; gray dot: trivial multiplier  $\lambda_{4K} = 1$ ); (c) snapshots of the instantaneous phases of the oscillators at time moments  $t_1 = 85$ ,  $t_2 = 120$ ,  $t_3 = 186$ ,  $t_4 = 214$ , with arrows indicating the direction of motion. Parameters:  $N = 11$ ,  $\mu = 1.0$ ,  $\varepsilon_1 = 1.0$ ,  $\alpha_1 = 1.7$ ,  $\varepsilon_2 = 0.129$ ,  $\alpha_2 = 1.72$ .

system (1). The initial phases  $\theta_k$  were chosen randomly from a uniform distribution on the interval  $[-\pi, \pi]$ , and the

velocities  $\dot{\theta}_k$  from the interval  $[-1, 1]$ . According to the obtained results, it can be seen that the dominant states are breathing and rotobreathing cyclops states. This confirms that in the investigated ensembles of phase oscillators, nonstationary three-cluster configurations possess wide basins of attraction and are typical attractors of the system.

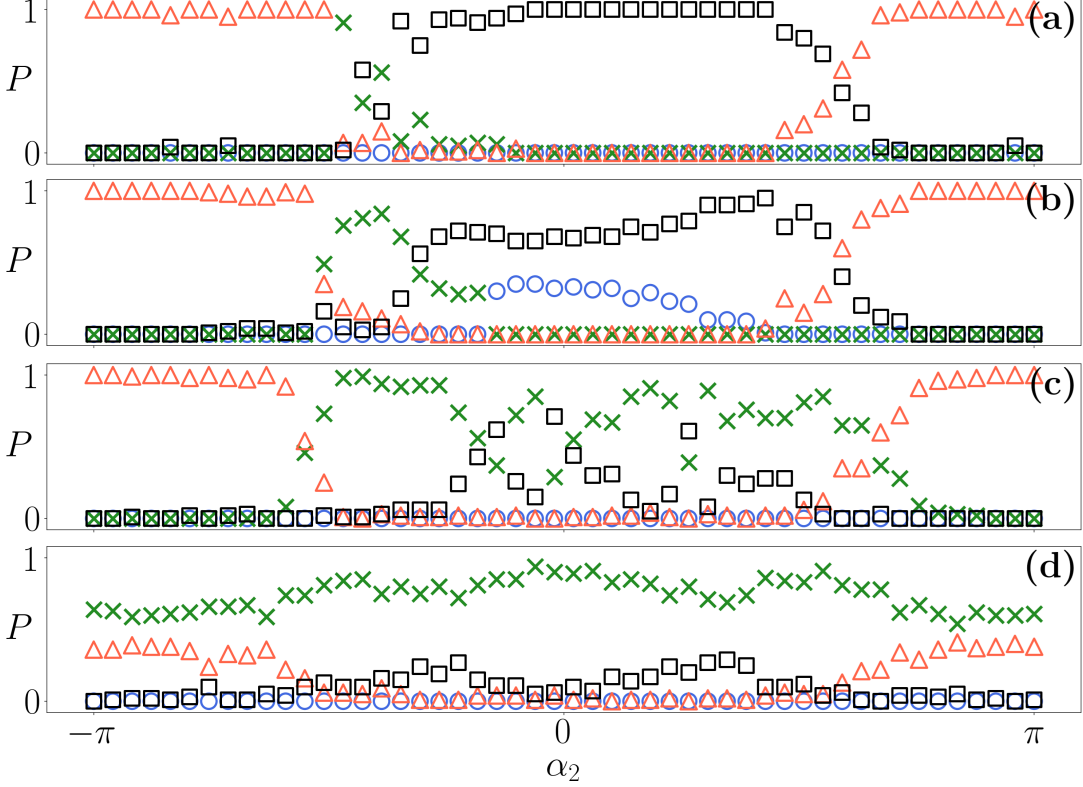


Figure 10. Probabilities  $P$  of realizing different dynamical states as functions of  $\alpha_2$  for fixed values of  $\varepsilon_2$ . Blue circles, green crosses, red triangles, and black squares indicate stationary cyclops, breathing, rotobreathing, and other states (including switching and multicluster states), respectively. Initial conditions were drawn randomly from uniform distributions:  $\theta_k \in [-\pi, \pi]$  and  $\dot{\theta}_k \in [-1, 1]$ . Parameters:  $N = 11$ ,  $\mu = 1.0$ ,  $\varepsilon_1 = 1.0$ ,  $\alpha_1 = 1.7$ ; (a)  $\varepsilon_2 = 0.15$ , (b)  $\varepsilon_2 = 0.1$ , (c)  $\varepsilon_2 = 0.05$ , (d)  $\varepsilon_2 = 0.01$ .

## VI. CONCLUSION

In the present work, a comprehensive analysis of nonstationary cyclops states in ensembles of phase oscillators with inertia and a two-harmonic coupling function has been carried out. Cyclops states are three-cluster configurations consisting of two coherent clusters and one solitary oscillator, and they are the dominant states in systems with an odd number of elements over a wide range of parameters, including the region of weak attraction and repulsion [23].

The main focus was on breathing and rotobreathing cyclops states, which preserve the three-cluster structure, unlike switching cyclops states. Using a reduction to a three-cluster manifold, it was established that breathing and rotobreathing cyclops states correspond to periodic and rotatory trajectories of the reduced system. The stability analysis revealed two main scenarios for the destabilization of nonstationary cyclops states.

The first scenario is associated with a period doubling, in which the three-cluster phase configuration is disrupted; however, the intra-cluster frequency synchronization is preserved, and the phase spreads remain small. It is proposed to classify the states emerging in this case as quasicyclops states. The second scenario is caused by the destabilization of one of the clusters, which leads to its disintegration into separate parts and a subsequent rearrangement of the cyclops configuration into a multicluster one.

Thus, the obtained results show that nonstationary cyclops states (breathing and rotobreathing) are key elements of the dynamics of phase oscillator ensembles with multiple coupling harmonics. Together with the fully synchronous state, they determine the structure of the phase space in a wide range of parameters. The proposed approach to the stability analysis and classification of cyclops states can be extended to more complex networks, including systems with nonpairwise interactions and adaptive coupling, as well as to models of neuronal dynamics, such as networks of theta neurons.

## ACKNOWLEDGMENTS

This work was supported by the RSF under Project No. 22-12-00348-P (model formulations and cluster reduction, breathing cyclops states, Sections II and III), and Project No. 24-72-00105 (rotobreathing cyclops states, statistical analysis, Sections IV and V).

- 
- [1] F. C. Hoppensteadt and E. M. Izhikevich, *Weakly Connected Neural Networks* (Springer, 2012).
  - [2] M. R. Tinsley, S. Nkomo, and K. Showalter, *Nat. Phys.* **8**, 662 (2012).
  - [3] J. Ding, I. Belykh, A. Marandi, and M.-A. Miri, *Phys. Rev. Appl.* **12**, 054039 (2019).
  - [4] F. Dörfler, M. Chertkov, and F. Bullo, *Proc. Natl. Acad. Sci. USA* **110**, 2005 (2013).
  - [5] A. E. Motter, S. A. Myers, M. Anghel, and T. Nishikawa, *Nat. Phys.* **9**, 191 (2013).
  - [6] Y. Kuramoto, in *International Symposium on Mathematical Problems in Theoretical Physics* (1975), p. 420.
  - [7] S. H. Strogatz, *Physica D* **143**, 1 (2000).
  - [8] B. Ermentrout and M. Lewis, *Bull. Math. Biol.* **59**, 533 (1997).
  - [9] J. A. Acebrón et al., *Rev. Mod. Phys.* **77**, 137 (2005).
  - [10] E. Ott and T. M. Antonsen, *Chaos* **18**, 037113 (2008).
  - [11] Y. Kuramoto and D. Battogtokh, *Nonlinear Phenom. Complex Syst.* **5**, 380 (2002).
  - [12] D. M. Abrams and S. H. Strogatz, *Phys. Rev. Lett.* **93**, 174102 (2004).
  - [13] M. J. Panaggio and D. M. Abrams, *Nonlinearity* **28**, R67 (2015).
  - [14] I. V. Belykh, B. N. Brister, and V. N. Belykh, *Chaos* **26**, 094822 (2016).
  - [15] B. N. Brister, V. N. Belykh, and I. V. Belykh, *Phys. Rev. E* **101**, 062206 (2020).
  - [16] P. Jaros, Y. Maistrenko, and T. Kapitaniak, *Phys. Rev. E* **91**, 022907 (2015).
  - [17] Y. Maistrenko et al., *Phys. Rev. E* **95**, 010203(R) (2017).
  - [18] V. O. Munyayev et al., *Phys. Rev. E* **105**, 024203 (2022).
  - [19] R. Delabays, *Chaos* **29**, 113129 (2019).
  - [20] M. Komarov and A. Pikovsky, *Phys. Rev. Lett.* **111**, 204101 (2013).
  - [21] P. S. Skardal, E. Ott, and J. G. Restrepo, *Phys. Rev. E* **84**, 036208 (2011).
  - [22] R. Berner, S. Yanchuk, Y. Maistrenko, and E. Schöll, *Chaos* **31**, 073128 (2021).
  - [23] V. O. Munyayev et al., *Phys. Rev. Lett.* **130**, 107201 (2023).
  - [24] M. I. Bolotov et al., *Phys. Rev. E* **109**, 054202 (2024).
  - [25] M. I. Bolotov et al., *Phys. Rev. E* **112**, 052202, (2025).
  - [26] H. Sakaguchi and Y. Kuramoto, *Prog. Theor. Phys.* **76**, 576 (1986).